

Creating Hemodynamic Atlases of Cardiac 4D Flow MRI

Merih Cibis, PhD,^{1,2*} Mariana Bustamante, MSc,^{1,2} Jonatan Eriksson, PhD,¹
Carl-Johan Carlhäll, MD, PhD,^{1,2,3} and Tino Ebbers, PhD^{1,2}

Purpose: Hemodynamic atlases can add to the pathophysiological understanding of cardiac diseases. This study proposes a method to create hemodynamic atlases using 4D Flow magnetic resonance imaging (MRI). The method is demonstrated for kinetic energy (KE) and helicity density (H_d).

Materials and Methods: Thirteen healthy subjects underwent 4D Flow MRI at 3T. Phase-contrast magnetic resonance cardioangiographies (PC-MRCAs) and an average heart were created and segmented. The PC-MRCAs, KE, and H_d were nonrigidly registered to the average heart to create atlases. The method was compared with 1) rigid, 2) affine registration of the PC-MRCAs, and 3) affine registration of segmentations. The peak and mean KE and H_d before and after registration were calculated to evaluate interpolation error due to nonrigid registration.

Results: The segmentations deformed using nonrigid registration overlapped (median: 92.3%) more than rigid (23.1%, $P < 0.001$), and affine registration of PC-MRCAs (38.5%, $P < 0.001$) and affine registration of segmentations (61.5%, $P < 0.001$). The peak KE was 4.9 mJ using the proposed method and affine registration of segmentations ($P = 0.91$), 3.5 mJ using rigid registration ($P < 0.001$), and 4.2 mJ using affine registration of the PC-MRCAs ($P < 0.001$). The mean KE was 1.1 mJ using the proposed method, 0.8 mJ using rigid registration ($P < 0.001$), 0.9 mJ using affine registration of the PC-MRCAs ($P < 0.001$), and 1.0 mJ using affine registration of segmentations ($P = 0.028$). The interpolation error was $5.2 \pm 2.6\%$ at mid-systole, $2.8 \pm 3.8\%$ at early diastole for peak KE; $9.6 \pm 9.3\%$ at mid-systole, $4.0 \pm 4.6\%$ at early diastole, and $4.9 \pm 4.6\%$ at late diastole for peak H_d . The mean KE and H_d were not affected by interpolation.

Conclusion: Hemodynamic atlases can be obtained with minimal user interaction using nonrigid registration of 4D Flow MRI.

Level of Evidence: 2

Technical Efficacy: Stage 1

J. MAGN. RESON. IMAGING 2017;46:1389–1399.

Several myocardial and heart valve diseases are characterized by abnormalities in heart anatomy concomitant with altered hemodynamics.^{1–4} Previous studies have demonstrated that in patients with cardiac diseases such as cardiomyopathy, valvular regurgitation, and conduction disorders, the intraventricular flow patterns are deranged, including impaired vortex formation^{5–7} and altered kinetic energy profiles.^{8,9} Similar abnormalities are also observed in other hemodynamic parameters, which could contribute to the progression of ventricular remodeling and dysfunction.^{10–14} Visualization and

quantification of intracardiac blood flow and the derived hemodynamic parameters are therefore essential to evaluate cardiac function and dysfunction.^{12,15,16} One of the emerging techniques that enables visualization and quantification of cardiac blood flow is 4D Flow magnetic resonance imaging (MRI), which provides time-resolved three-directional blood flow information.^{17–19} The reduction of scan time introduced by new acceleration techniques has already led to an increase in the number of studies based on this type of acquisition.^{20–22} With further improvements in acquisition and data processing

View this article online at wileyonlinelibrary.com. DOI: 10.1002/jmri.25691

Received Dec 7, 2016, Accepted for publication Feb 14, 2017.

*Address reprint requests to: M.C., Linköping University, Division of Cardiovascular Medicine, Department of Medical and Health Sciences, SE-581 85 Linköping, Sweden. E-mail: merih.cibis@liu.se

From the ¹Division of Cardiovascular Medicine, Department of Medical and Health Sciences, Linköping University, Linköping, Sweden; ²Center for Medical Image Science and Visualization (CMIV), Linköping University, Linköping, Sweden; and ³Division of Clinical Physiology, Department of Medical and Health Sciences, Linköping University, Linköping, Sweden

This is an open access article under the terms of the Creative Commons Attribution-NonCommercial License, which permits use, distribution and reproduction in any medium, provided the original work is properly cited and is not used for commercial purposes.

Additional Supporting Information may be found in the online version of this article.

techniques, one can expect that 4D Flow MRI will continue to develop in both research and clinical settings.

Although 4D Flow MRI data provides valuable information, its analysis is challenging when a group of subjects are studied. In most of the 4D Flow MRI studies, the data are either visualized individually, or the cardiac flow is simplified to a single or a few values.^{3,11,23} While the former approach is not feasible for the studies with more than a few subjects, the latter does not represent the full 4D behavior of the cardiac flow. In an alternative approach, 4D Flow MRI data can be analyzed by obtaining hemodynamic atlases. Some attempts have been made to obtain hemodynamic atlases based on 4D Flow MRI in large vessels.^{24,25} Van Ooij et al introduced a method to derive a 3D wall shear stress (WSS) atlas in the aorta using 4D Flow MRI.²⁴ In their study, the aortas of a group of subjects were segmented and aligned with a cohort-specific aorta geometry using affine registration. After projecting the WSS values, the average and the standard deviation of the WSS were quantified. In another study, Van Ooij et al obtained the WSS distribution of patients with bicuspid aortic valve disease and the aortic WSS atlas of a healthy population.²⁵ They found that the regions of elevated WSS in these patients relative to the healthy WSS atlas coincide with the aortic regions to be resected. Their approach might be extended to obtain the atlases of similar hemodynamic parameters in other great vessels and also in the heart. However, segmentation of each individual subject is necessary for this approach, which is not feasible for studies conducted with a larger number of subjects, and is very challenging for cardiac 4D Flow MRI data. In addition, the global registration methods such as rigid and affine registration can result in insufficient alignment of anatomical structures, resulting in a severe smoothing of the averaged images. While rigid registration performs a global transformation of the images by translation and rotation, affine registration additionally includes scaling and shearing, which results in a global deformation. On the other hand, nonrigid registration performs elastic deformations and local alignment of anatomical features.²⁶ To obtain hemodynamic atlases with higher quality, the use of more advanced methods such as nonrigid registration is expected to be necessary.

In this study, the aim is to obtain more accurate hemodynamic atlases of 4D Flow MRI images with minimal user interaction using nonrigid deformation.

Materials and Methods

Study Population and MR Examination

Thirteen healthy subjects (eight females and five males, 31 ± 12 years, resting heart rate 64 ± 9 bpm) with no prior or current cardiovascular disease were included in the study. All subjects gave informed consent and the study was approved by the Regional Ethical Review Board.

These subjects underwent cardiac MRI on a clinical 3T MR scanner (Philips Achieva, Phillips Medical Systems, Best, The

Netherlands) using a 32-element phased-array coil system. The MR protocol included 4D Flow MRI of the left heart and the morphological long and short axis data of the left ventricle (LV) without contrast agent. Data were acquired during free breathing using retrospective ECG and respiratory gating. The 4D Flow MRI acquisition parameters included velocity encoding (venc) 120–150 cm/s, flip angle 5° , repetition time 5.2 msec, echo time 3 msec, echo train length 2, spatial resolution $2.7 \times 2.7 \times 2.7 \text{ mm}^3$, field of view $300 \times 300 \times 120 \text{ mm}^3$, parallel imaging (SENSE) with a reduction factor of 3 and a k -space segmentation factor of 2. For the navigator gating, an adaptive acceptance window ranging between 5 mm and 20 mm was used. The navigator gated scans were ~ 15 minutes. The effective temporal resolution was 41.6 msec and the velocity data were reconstructed into 40 time frames. The data were corrected for concomitant gradient fields on the scanner. The postprocessing included correction for phase wraps using a temporal phase unwrapping method,²⁷ and correction for eddy-current distortions using a weighted second order fit to static tissue.

Temporal Alignment

4D phase contrast magnetic resonance cardioangiographies (PC-MRCAs) were created, by combining 4D Flow MRI magnitude and velocity data. The PC-MRCAs are the improved, time-resolved phase contrast MR angiograms obtained by registering different time frames. A brief description of the process is included in Supplemental Material Appendix A. The details of creating PC-MRCAs are described elsewhere.²⁸ The mid-systolic time frame, defined as the time frame of peak flow over the aortic valve, and the early and late diastolic time frames, defined as the time frames of the two consecutive peak flows observed in the mitral valve, were found by using the velocities measured by the 4D Flow MRI. The PC-MRCAs were temporally aligned at the time frames of mid-systole, early diastole, and late diastole. The intermediate time frames between mid-systole, early and late diastole were linearly interpolated, resulting in 40 time frames per cardiac cycle. The temporal alignment was visually inspected by plotting flow waveform of each individual after registration to the average heart.

Creating an Average Heart

First, the PC-MRCAs were rigidly registered to one of the subjects, referred to as "Subject 1." The PC-MRCA of Subject 1 was then nonrigidly registered to all PC-MRCAs to obtain 4D deformation fields.²⁹ The deformation fields obtained from the registrations were averaged and applied to the PC-MRCA of Subject 1, which resulted in a time-resolved 3D data referred to as "average heart." The workflow to create the average heart is shown in Fig. 1. The LV, left atrium (LA), and ascending aorta of the average heart were manually segmented by one researcher (M.C.) at mid-systole, early and late diastole using the open source software ITK-SNAP.³⁰

Registration of Each Individual Dataset to the Average Heart

After creating the average heart, the PC-MRCAs were nonrigidly registered to the average heart. The deformations obtained from these registrations were then applied to the manual segmentations on the PC-MRCAs.

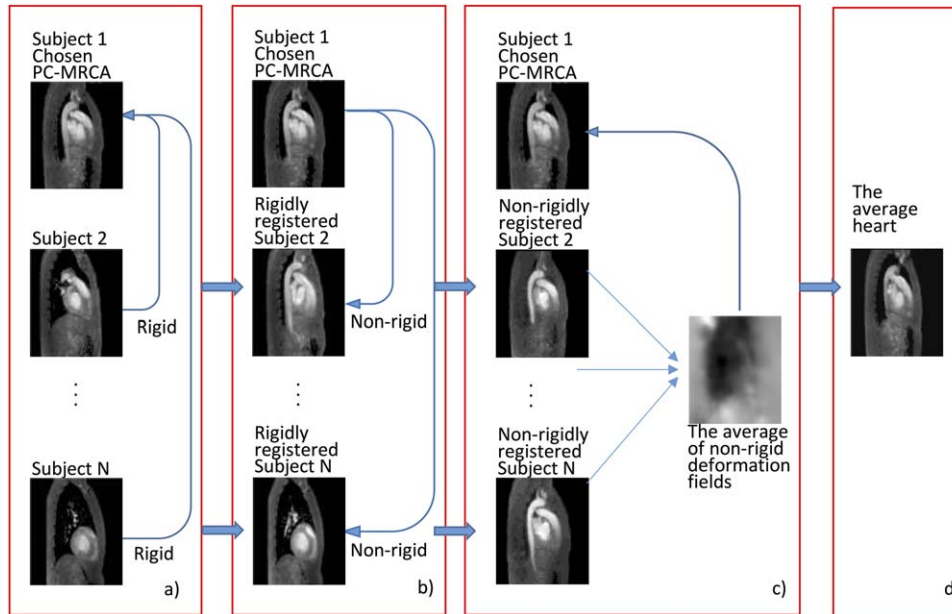


FIGURE 1: Workflow to create the time-resolved average heart. (a) The individual PC-MRCAs were rigidly registered to the PC-MRCA of Subject 1. (b) The PC-MRCA of Subject 1 was nonrigidly registered to all PC-MRCAs which were rigidly registered in the previous step. (c) The deformation fields obtained were averaged and applied to the PC-MRCA of Subject 1. (d) The time-resolved average heart is obtained as a result.

The nonrigid registrations were executed using the Morphon method.^{31,32} Morphon method deforms a prototype image into a target image by estimating the local displacements to make the prototype image similar to the target image. The Morphon method continues deformation in an iterative manner, but fluid and elastic regularizations constrain the deformation permitted in order to generate plausible transformations.³³ The registrations were performed using three scales (2.7 mm, 5.4 mm, 10.8 mm), five iterations per scale, and linear interpolation, which were optimized by evaluating different parameters and the computational cost.

All registrations were performed using an in-house software package implemented in MatLab (MathWorks, Natick, MA) on a desktop computer (Intel Xeon 12 core processors, 2.50 GHz CPU, and 64 GB RAM). The registration took ~ 2 minutes per time frame. The total computational time for creating the average heart and registering individual subjects to the average heart for all time frames was ~ 20 hours.

Kinetic Energy and Helicity Density Atlases

The proposed method was demonstrated by creating the atlases of intracardiac kinetic energy (KE) and helicity density (H_d), which are flow parameters previously associated with several cardiovascular diseases such as ventricular remodeling, aortic and mitral valve regurgitation, and aortic dilatation.^{8,9,12,15,34,35} KE and H_d were derived from the 4D Flow MRI velocities. KE was calculated per voxel as:

$$KE = \frac{1}{2} \rho v^2 dV \quad (1)$$

where ρ is the blood density, dV is the unit voxel volume, and v is the speed of blood. The blood density was assumed to be 1060 kg/m^3 . H_d was calculated as:

$$H_d = \vec{u} \cdot \text{curl}(\vec{u}) \quad (2)$$

where \vec{u} is the velocity in three directions, and $\text{curl}(\vec{u})$ is the vorticity per voxel. These parameters were calculated before registration to the average heart. The deformation fields obtained using the nonrigid registrations were applied to the intensity images representing the hemodynamic parameters. These deformations were performed using cubic interpolation. The registered hemodynamic parameters were then averaged to obtain the hemodynamic atlases. The workflow to obtain the KE atlas is shown in Fig. 2, which also represents the workflow to generate the H_d atlas.

Evaluation

The proposed method, which uses nonrigid registration to create hemodynamic atlases, was compared with those based on rigid and affine registration. The LV, LA, and the ascending aorta of each individual subject at early diastole were segmented from the PC-MRCAs before registration. These segmentations were deformed using the deformation field obtained by nonrigid registration of the PC-MRCAs to the average heart. The segmentations deformed nonrigidly were compared with the same segmentations deformed using 1) rigid registration of the PC-MRCAs to the average heart, 2) affine registration of the PC-MRCAs to the average heart, and 3) affine registration of the segmentations to the segmentation of the average heart.

The overlap volume between the deformed individual segmentations and the segmentation of the average heart was calculated and normalized with the volume of the average heart segmentation. The registration accuracy was evaluated by calculating the median and the interquartile range (IQR) of the overlap volumes in percentages.

The effect of the registration method on the derived parameters was investigated for the KE at early diastole by comparing the derived atlases using the registration methods described above. The

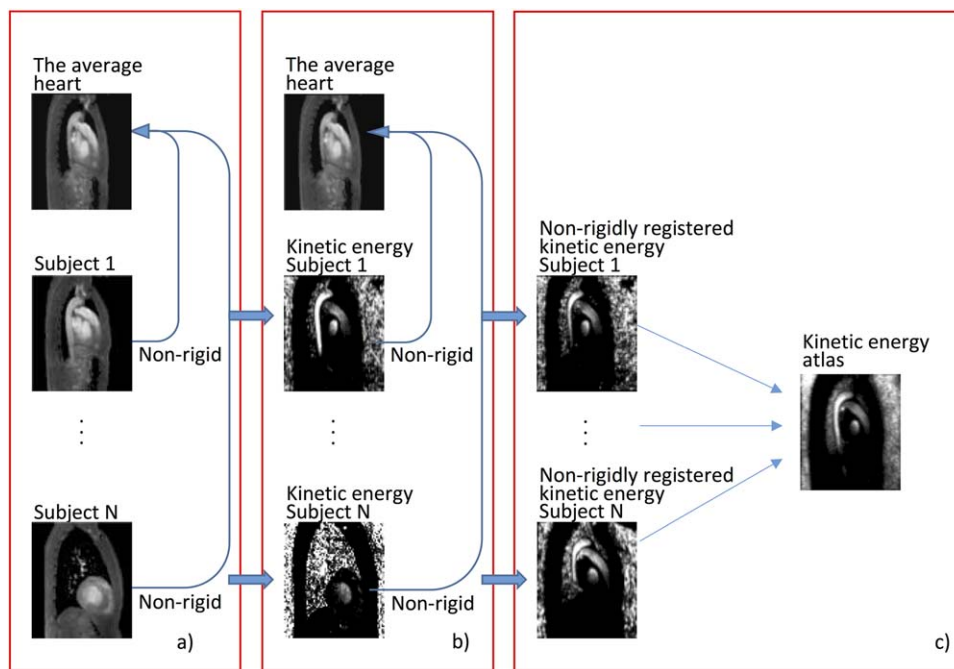


FIGURE 2: Workflow to calculate the kinetic energy (KE) atlas. (a) The individual PC-MRCAs were nonrigidly registered to the average heart. (b) The KE images were also nonrigidly registered to the average heart by using the deformation fields obtained from part (a). (c) The nonrigidly registered kinetic energy images were averaged and the kinetic energy atlas was obtained.

peak (99th percentile) and the mean values of the KE atlases obtained by using different registration methods were compared. The KE and H_d atlases were shown as maximum intensity projection (MIP) images in three orientations or in a single slice. The averaged deformation field was also included to show the heterogeneity of the left heart anatomy within this group of healthy subjects.

The effect of change in the population size on the hemodynamic atlases was evaluated by performing Monte Carlo simulations. The mean and peak KE of KE atlases based on all possible subsets of the study population ($n = 8191$) were calculated at mid-systole, early diastole, and late diastole using nonrigid registration of the PC-MRCAs. The results are presented as histogram plots.

The interpolation error resulting from the nonrigid registration was assessed at mid-systole, early diastole, and late diastole by comparing the peak and mean KE and H_d of each subject before and after registration to the average heart. The values are represented as mean \pm standard deviation.

The registration accuracy of different methods was assessed using Wilcoxon signed-rank test and the interpolation error in peak and mean KE and H_d were assessed using a paired t -test, and a significance level of $P < 0.05$ was considered statistically significant.

Results

In Fig. 3a, MIPs of the KE atlas obtained using the proposed method are shown at mid-systole, early diastole, and late diastole. The KE was found highest in the aorta at mid-systole. At early diastole, the KE was lower, and the peak KE was close to the mitral valve in the LV. At late diastole, the KE was even lower, and the highest KE was observed in

the vicinity of the left atrial appendage (LAA) inlet, possibly caused by flow from the LAA into the LA. The standard deviation of the KE was higher in the regions of higher mean KE. Figure 3b illustrates the mean KE over one cardiac cycle. Figure 4 shows the KE atlas, the standard deviation, and the average deformation field in a single slice at early diastole. The deformation field shows that the apical half of the LV, the posterior part of the LA, and the proximal ascending aorta had the most anatomical variety between subjects.

The H_d atlas and the standard deviation of the H_d obtained using the proposed method are shown in Fig. 5a. The absolute magnitude of H_d was found to be highest in the aorta at mid-systole, and in the LV at early diastole. At late diastole, the absolute magnitude of H_d was lower. Figure 5b shows the mean of the absolute values of H_d over one cardiac cycle. Time-resolved, 3D movies of the KE and H_d atlases are provided as online Supplementary Material.

Evaluation

All PC-MRCAs were successfully registered to the average heart. Figure 6 shows the overlap of the manual segmentations deformed using (Fig. 6a) nonrigid, (b) rigid, (c) affine registration of the PC-MRCAs, and (d) affine registration of the manual segmentations. The median and IQR of the overlap volume were 92.3% and 61.5% for nonrigid registration, which was higher than those obtained for rigid registration of the PC-MRCAs (23.1% and 46.1%, $P < 0.001$), affine registration of the PC-MRCAs (38.5% and 61.5%, $P < 0.001$),

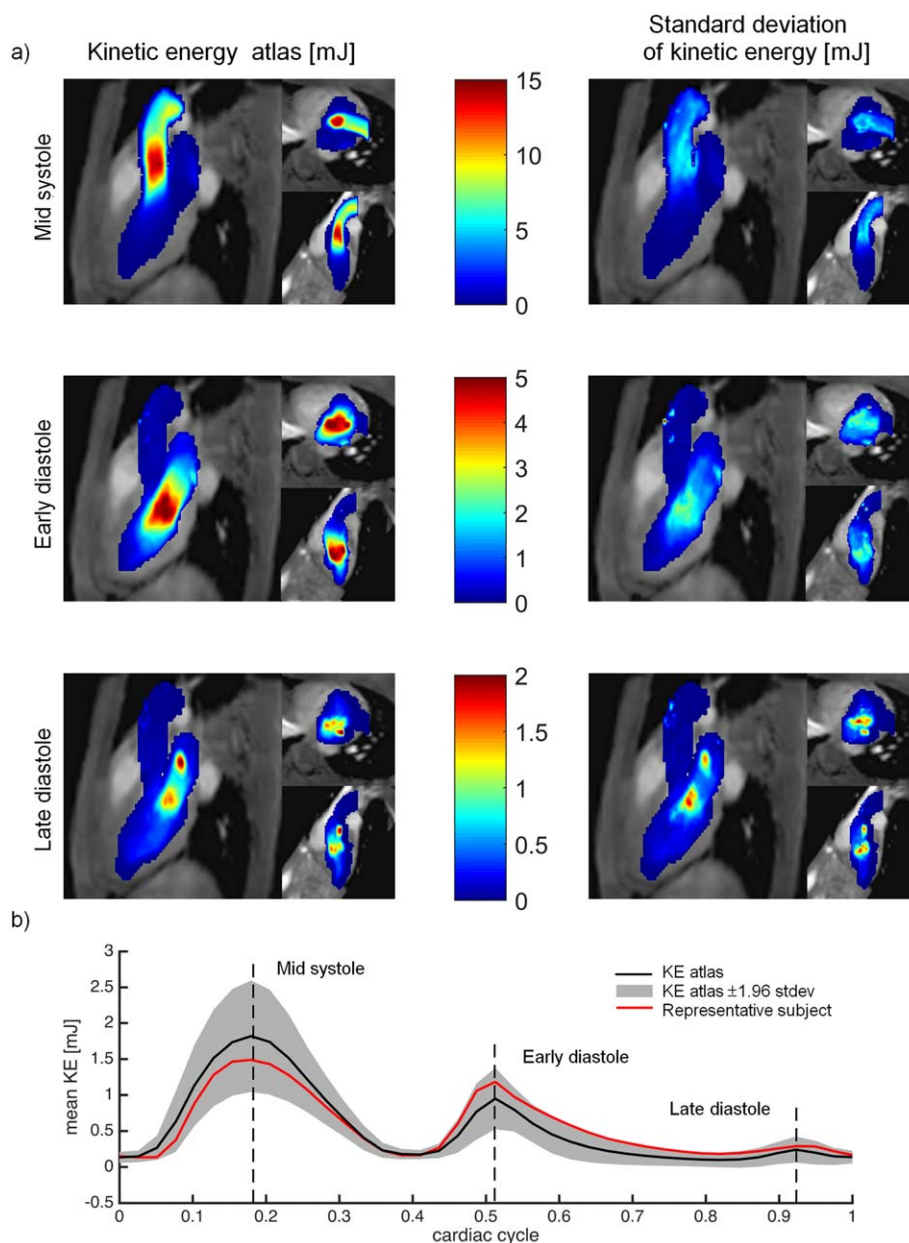


FIGURE 3: (a) MIPs of the kinetic energy atlas (KE) (mJ) generated by the proposed method. The results are shown in three orientations: three-chamber view, short-axis view, and two-chamber view. Top: mid-systole, middle: early diastole; and bottom: late diastole. Left: KE atlas, right: standard deviation of the KE. (b) Mean KE throughout the cardiac cycle. The black line shows the mean value of the KE atlas, the gray area shows the KE atlas ± 1.96 standard deviation, and the red line shows the mean KE of a representative subject.

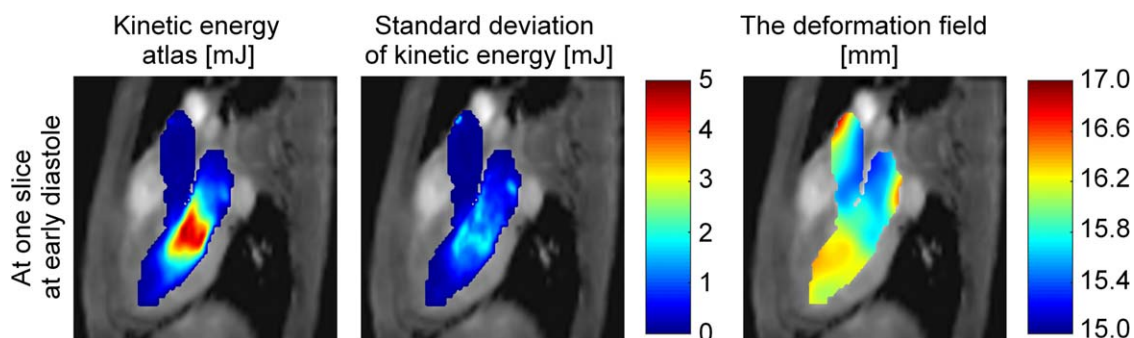


FIGURE 4: Kinetic energy atlas (KE) (mJ), standard deviation of KE (mJ), and the averaged deformation field in a single slice generated by the proposed method using nonrigid registration.

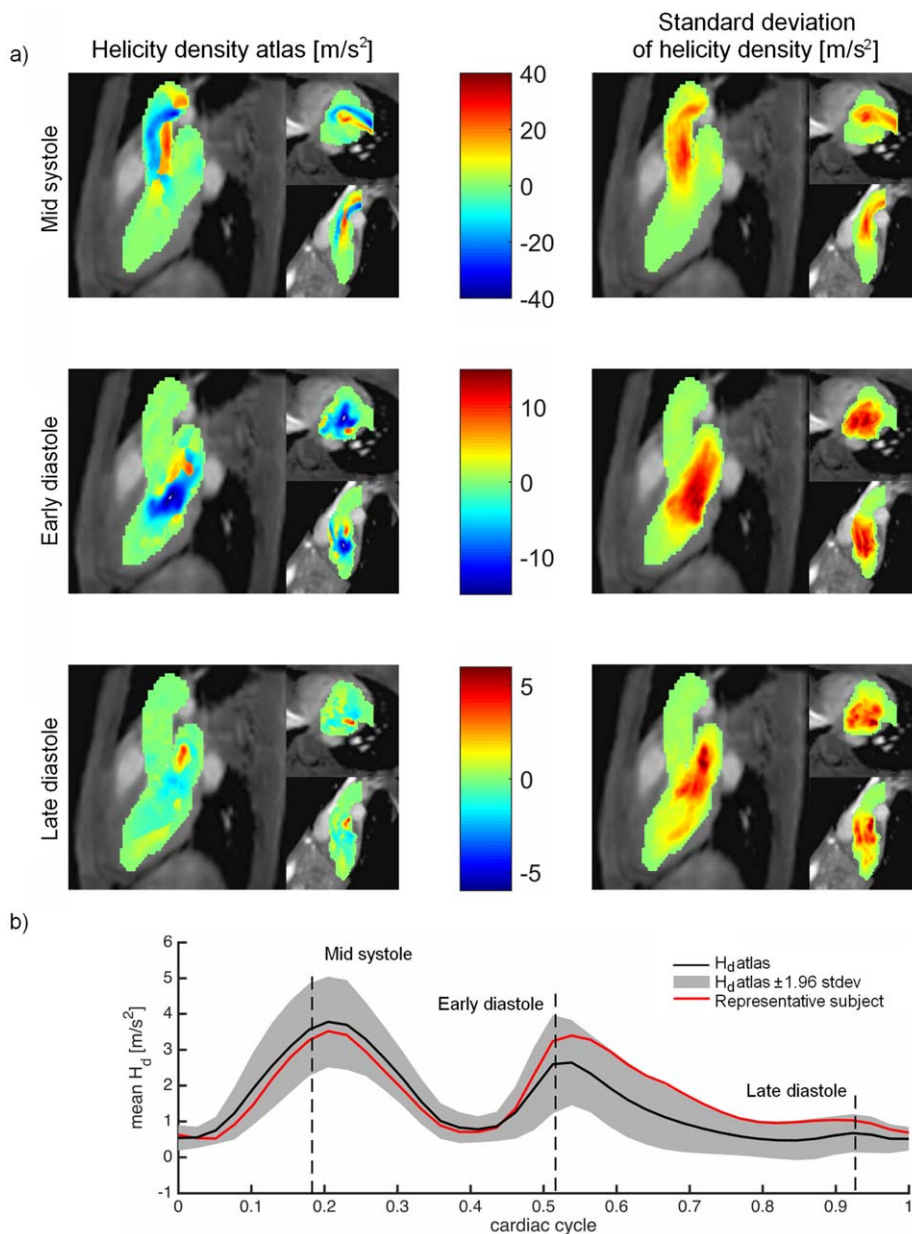


FIGURE 5: (a) MIPs of the helicity density (H_d) atlas (m/s^2) generated by the proposed method. The results are shown in three orientations: three-chamber view, short-axis view, and two-chamber view. Top: mid-systole, middle: early diastole; and bottom: late diastole. Left: mean H_d , right: standard deviation of the H_d . (b) Mean H_d throughout the cardiac cycle. The black line shows the mean value of the H_d atlas, the gray area shows the H_d atlas ± 1.96 standard deviation, and the red line shows the mean H_d of a representative subject. Note that mean values were calculated using the absolute magnitude of H_d .

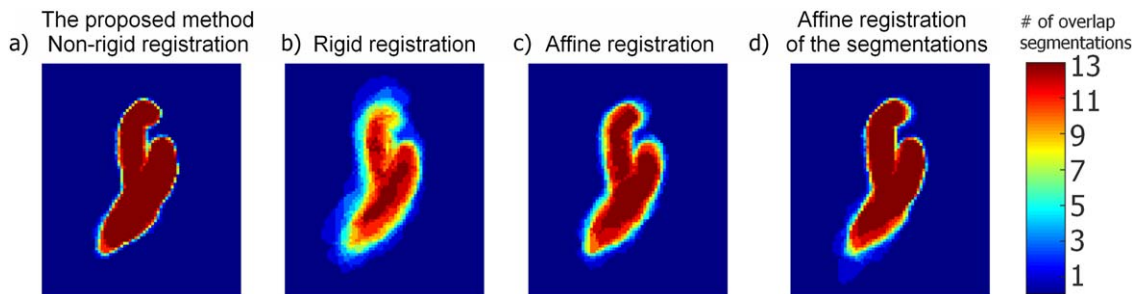


FIGURE 6: The MIP of the overlapping segmentations which were deformed using (a) nonrigid registration of the PC-MRCAs, (b) rigid registration of the PC-MRCAs, (c) affine registration of the PC-MRCAs, (d) affine registration of the manual segmentations. The color bar shows the number of overlapping segmentations.

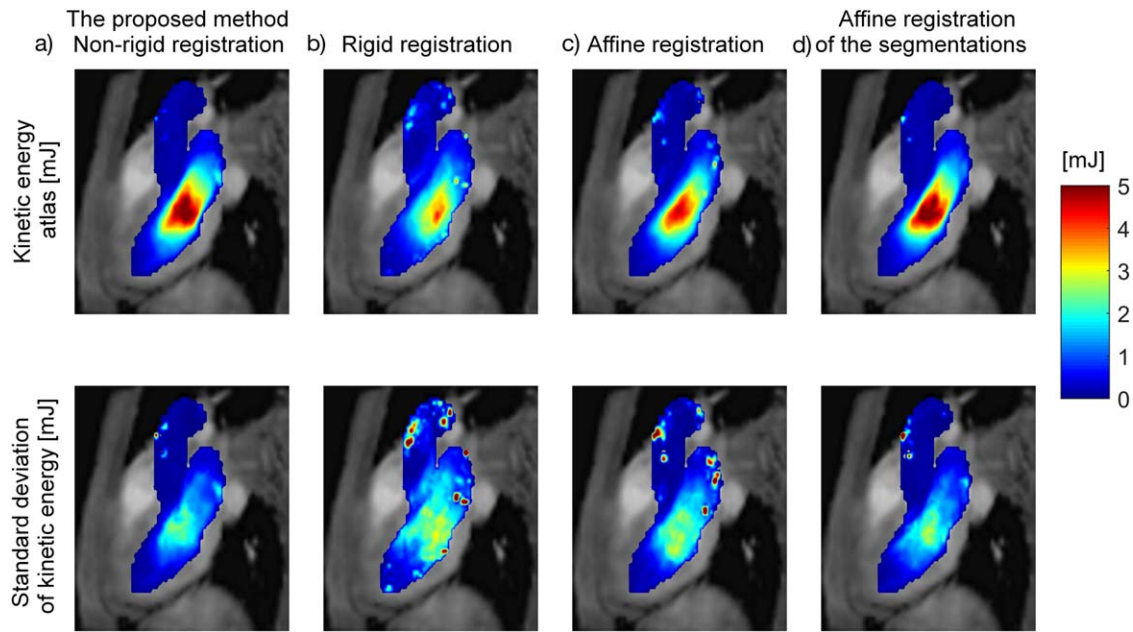


FIGURE 7: Top row: The kinetic energy atlas and bottom row: the standard deviation at early diastole obtained using (a) nonrigid registration of the PC-MRCAs, (b) rigid registration of the PC-MRCAs, (c) affine registration of the PC-MRCAs, (d) affine registration of the manual segmentations.

and affine registration of the segmentations (61.5% and 84.6%, $P < 0.001$).

Figure 7 shows the MIP of the KE atlases at early diastole based on (Fig. 7a) nonrigid, (b) rigid, (c) affine registration of the PC-MRCAs, and (d) affine registration of the manual segmentations. The mean of the KE atlas obtained using nonrigid registration of the PC-MRCAs (1.1 mJ) was significantly higher than that obtained using rigid registration of the PC-MRCAs (0.8 mJ, $P < 0.001$), affine registration of the PC-MRCAs (0.9 mJ, $P < 0.001$), and affine registration of the segmentations (1.0 mJ, $P = 0.028$). The peak of the KE atlas obtained using nonrigid registration of the PC-MRCAs (4.9 mJ) was similar to that obtained using affine registration of the segmentations (4.9 mJ, $P = 0.91$), but higher than the affine registration (4.2 mJ, $P < 0.001$) and rigid registration (3.5 mJ, $P < 0.001$) of the PC-MRCAs. The rigid and affine registration of the PC-MRCAs also resulted in higher standard deviation of the KE (mean 0.9 mJ and 0.8 mJ, respectively) relative to the nonrigid registration of the PC-MRCAs (mean 0.6 mJ, $P < 0.001$) and the affine registration of the segmentations (mean 0.6 mJ, $P < 0.001$). The overlap of the deformed segmentations as well as the mean and peak KE and H_d were calculated for LA and LV separately using different registration methods which can be found in Appendix B.

The histogram plots showing the mean and peak KE of the KE atlases based on all possible subsets of the study population are presented in Fig. 8. The mean KE of all possible KE atlases was 2.2 ± 0.1 mJ at mid-systole, 1.1 ± 0.1 mJ at early diastole, and 0.2 ± 0.0 mJ at late diastole. The peak KE was 14.2 ± 0.9 mJ at mid-systole, 5.0 ± 0.5 mJ at

early diastole, and 1.7 ± 0.3 mJ at late diastole. The mean and peak KE of the largest subset ($n = 13$) was approximated with an accuracy of 10% for the subsets including more than seven subjects.

Figure 9 shows the MIP of the KE of a representative subject before and after nonrigid registration to the average heart. The results are presented at mid-systole, early diastole, and late diastole. As can be seen, the patterns of high and low KE remained similar after registering to the average heart, although the peak values decreased after the registration. These observations were also valid for H_d (data not shown). Table 1 shows the peak KE and H_d , the mean KE and H_d in the LV, and in the LA at mid-systole, early diastole, and late diastole before and after nonrigid registration. Note that the peak and mean H_d calculations are based on the absolute magnitude of the H_d . The peak KE was significantly underestimated after registration. The underestimation due to registration was $5.2 \pm 2.6\%$ at mid-systole ($P < 0.001$), and $2.8 \pm 3.8\%$ at early diastole ($P = 0.01$). No significant difference was found in peak KE before and after registration at late diastole ($P = 0.44$). The mean KE in the LV and LA remained the same after registration at all time frames. The peak H_d was underestimated after registration to the average heart. The underestimation was $9.6 \pm 9.3\%$ at mid-systole ($P = 0.006$), $4.0 \pm 4.6\%$ at early diastole ($P = 0.002$), and $4.9 \pm 4.6\%$ at late diastole ($P = 0.004$). The mean H_d values remained the same after registration.

Discussion

In this study a method was introduced to obtain 4D hemodynamic atlases using cardiac 4D Flow MRI, here

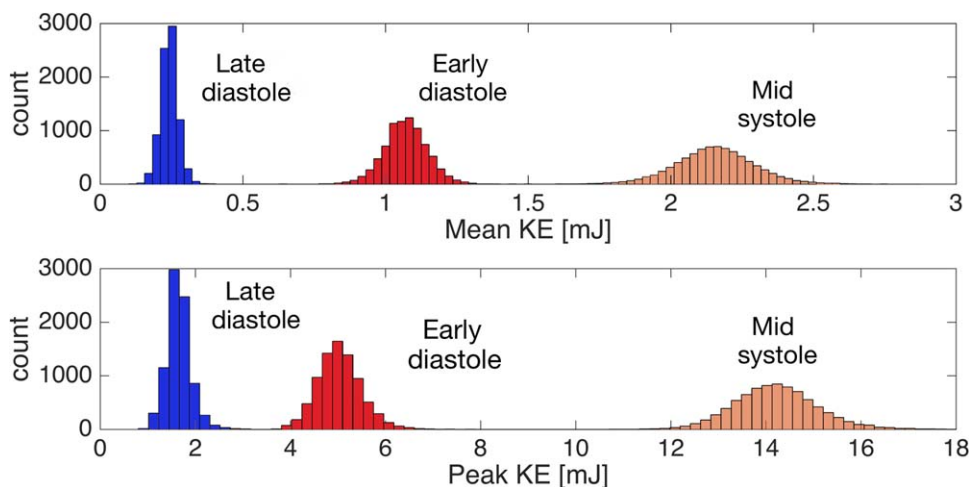


FIGURE 8: Histogram showing the mean (upper panel) and peak (lower panel) KE (mJ) for all possible KE atlases using the subsets of the study population ($n = 8191$) at mid-systole, early diastole and late diastole. The x-axis shows the KE (mJ) values and the y-axis shows the count of subsets.

demonstrated specifically for cardiac KE and H_d . The proposed method registers anatomical parts, hence reduces the morphological differences between subjects, which permits the calculation of hemodynamic atlases. The main

advantages of this method are that it enables improved atlas accuracy over rigid and affine registration-based atlases, it does not require segmentation of every subject, and it is automated. The nonrigid registrations were performed using

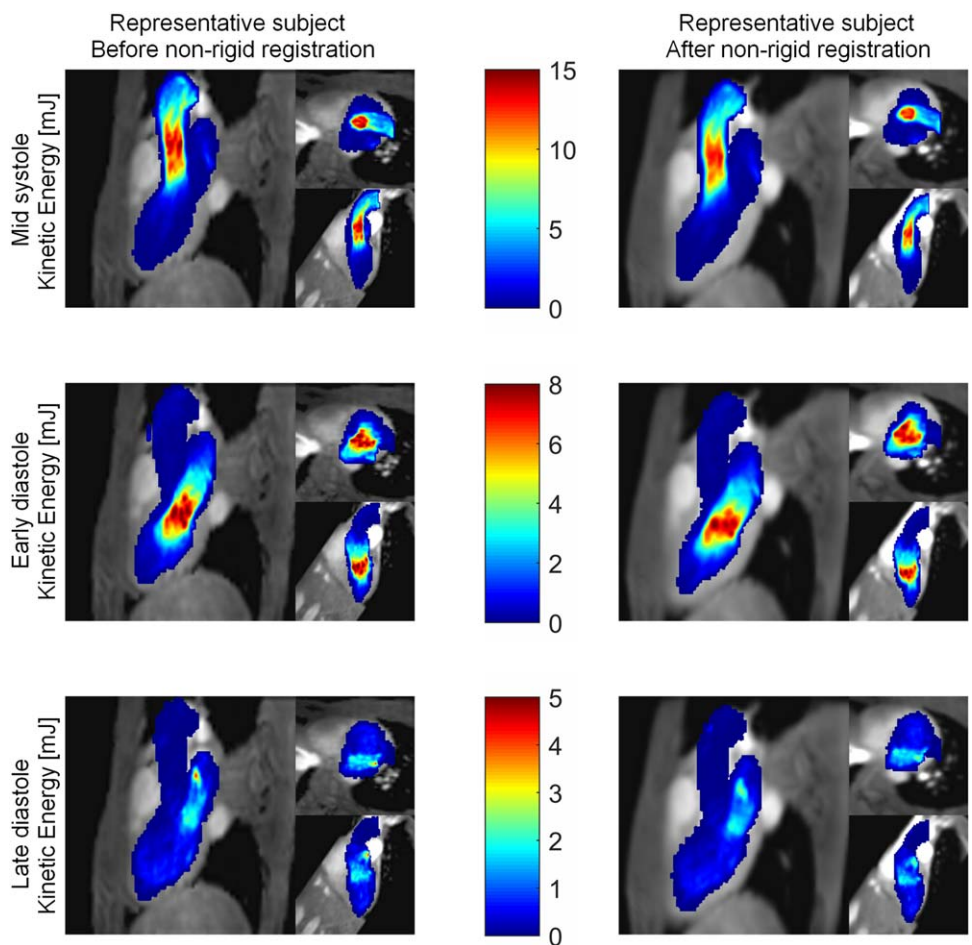


FIGURE 9: MIP of the kinetic energy (mJ) of one representative subject in three orientations: three-chamber view, short-axis view, and two-chamber view. Top: mid-systole, middle: early diastole, and bottom: late diastole. Left: before nonrigid registration, right: after nonrigid registration to the average heart.

the Morphon method, which has the main advantage of being robust and tolerant to grayscale variation between images.

The comparison between nonrigid and other registration methods showed that local alignment of anatomical features is necessary for a better estimation of the hemodynamic atlases. Although KE patterns could still be observed when rigid and affine registration were used, the values of the KE atlas, especially the peak values, were largely underestimated. In addition, the standard deviation values were found to be higher and more scattered. The nonrigid registration of anatomical features resulted in lower standard deviations, as well as higher values in the hemodynamic atlas. The KE atlas obtained using nonrigid registration of the PC-MRCAs resulted in a similar KE atlas to that obtained using affine registration of the manual segmentations. The latter approach, however, requires segmentation of each individual subject, which is a considerable disadvantage if segmentation is performed manually, and if a large number of subjects is included in the study.

The hemodynamic atlases and the standard deviations depend on both the anatomical alignment, and the temporal alignment of the heart phases. Temporal registration, which is performed to avoid intersubject variability between the heart phases, might fail in a large heterogeneous group of subjects. For a heterogeneous group, further subdivision of the subjects might be required according to their cardiac cycles. The spatial registration using the proposed method was evaluated by calculating the overlap of the deformed segmentations and was found to be above 90%. The registration accuracy would be dependent on the time frame that the registration was performed. It is expected to be lower at diastolic time frames in the LV due to lower blood velocities inside the heart, resulting in less contrast in the PC-MRCA data. The authors do not expect a major effect if the spatial and temporal resolution of the images are changed, but the registration accuracy increases by using artifact-free images with high signal-to-noise ratio, which might be reflected by lower standard deviations.

The proposed method was used to demonstrate the characteristics of blood flow in the left heart of healthy subjects. In this healthy group, the aortic root at mid-systole and the vicinity of the mitral valve at early diastole were found to be the regions with higher values of KE and low values of standard deviation in the generated atlas. Regions with elevated KE were also found in the KE atlas in the mid-ventricle at early diastole and late diastole, but with higher values of standard deviation, indicating that the KE in these regions varied in location and/or intensity within the group. The distribution of KE in the atlas was in agreement with the literature.^{11,14,36,37} For H_d , the LV outflow tract and aortic valve area showed high H_d with low standard deviations, showing that these findings are consistent

TABLE 1. Peak and Mean Kinetic Energy (KE) and Helicity Density (H_d) Before and After Registration to the Average Heart

	Mid systole			Early diastole			Late diastole		
	Before nonrigid registration	After nonrigid registration	P-value	Before nonrigid registration	After nonrigid registration	P-value	Before nonrigid registration	After nonrigid registration	P-value
Peak KE [mJ]	14.9 ± 2.8	14.2 ± 2.8*	<0.001	5.6 ± 1.3	5.4 ± 1.2*	0.02	1.7 ± 0.9	1.7 ± 0.9	0.93
Mean KE LV [mJ]	0.9 ± 0.2	0.9 ± 0.2	0.78	1.4 ± 0.4	1.5 ± 0.4	0.33	0.3 ± 0.2	0.3 ± 0.2	0.98
Mean KE LA [mJ]	0.3 ± 0.1	0.3 ± 0.1	0.18	1.2 ± 0.5	1.2 ± 0.5	0.59	0.4 ± 0.1	0.4 ± 0.2	0.41
Peak H_d [m ² /s ²]	36.4 ± 6.8	33.1 ± 8.3*	0.006	19.7 ± 5.2	18.9 ± 5.0*	0.002	4.8 ± 2.3	4.6 ± 2.3*	0.005
Mean H_d LV [m ² /s ²]	2.0 ± 0.4	2.0 ± 0.4	0.34	3.6 ± 1.4	3.4 ± 1.3	0.06	0.8 ± 0.3	0.7 ± 0.3	0.07
Mean H_d LA [m ² /s ²]	1.1 ± 0.3	1.2 ± 0.4	0.11	4.1 ± 1.4	4.1 ± 1.5	0.95	1.1 ± 0.6	1.1 ± 0.5	0.24

The peak kinetic energy (KE) and helicity density (H_d), and the mean KE and H_d in the LV and LA before and after registration to the average heart at mid systole, early diastole, and late diastole. Note that the peak and mean H_d values are based on the absolute values of the H_d .

*Significant difference between the values before and after nonrigid registration.

within the group. The magnitude of H_d was higher at the aortic valve area due to the curvature of the aortic arch.^{38,39} The standard deviation of H_d was higher towards the aortic arch, indicating larger variations between subjects in that region. Helicity density is a hemodynamic parameter with a \pm sign given according to the direction of the helical flow. In the areas of helical flow, ie, in the vicinity of mitral valve at early diastole, helical flow structures are observed in both directions.^{40,41} The spatial variation in the direction of the helical flow reduces the average helicity density in the atlas and increases the standard deviation, reflecting the variation of the parameter. The Monte Carlo simulations resulted in low standard deviations of the mean and peak KE, showing that the dependency of the results on the size of the group was small in healthy subjects. If a relatively small number of the subjects is included, the mean and peak kinetic energy values were slightly biased depending on the subjects included. As the number of subjects increased, ie, above seven, the effect of including/subtracting subjects was already decreasing, indicating that a relatively low number of subjects is sufficient to create an atlas for KE.

In this study we present and evaluate a novel method to create hemodynamic atlases in a healthy group. A healthy hemodynamic atlas provides information about the expected flow patterns, the range of the expected values, and the variability within healthy subjects. The comparison between healthy hemodynamic atlases and individual patients can be used to detect pathologies. Van Ooij et al used the healthy hemodynamic atlases of the aorta to detect the regions with abnormal blood flow in patients with a bicuspid aortic valve.²⁴ They assessed the size and the position of aortic regions with hemodynamic values deviating more than two standard deviations compared to the healthy hemodynamic atlas. Accordingly, a healthy hemodynamic cardiac atlas can be used as an additional diagnostic tool.

The hemodynamic atlases of different patient groups can also facilitate comparison of different groups of patients, or comparison of individual patients with patient atlases. A hemodynamic atlas of a patient group and its standard deviation can provide information about the variability of the hemodynamic parameters for a specific disease. The individual patients can be classified by evaluating the differences and similarities relative to the atlases. Future studies need to be conducted to create hemodynamic atlases for different patient cohorts.

The KE and the H_d were the only hemodynamic parameters evaluated in the left heart. However, the presented method is not restricted to these flow parameters, as it can be applied to almost any hemodynamic parameter, such as turbulent kinetic energy, energy loss, vorticity, speed, etc. In addition, the hemodynamic atlases can be created for the right heart as well as other large vessels.

Although nonrigid registration of the anatomical features is the strength of the method, it also leads to some limitations. The main disadvantages of nonrigid registration compared to rigid registration are that nonrigid registration has higher computational cost and possibly leads to more smoothing due to interpolation. When the registrations were applied, the intensity images representing the hemodynamic parameters were deformed and interpolated. The peak values of the hemodynamic parameters were therefore slightly underestimated ($5.2 \pm 2.6\%$ for KE and $9.6 \pm 9.3\%$ for H_d at mid-systole). Nevertheless, the mean values were not influenced by the registration. Note that the nonrigid registration was performed without taking conservation of mass and momentum into account. Consequently, the continuity equation might not be satisfied after the deformation fields were applied. One remedy might be to correct the hemodynamic parameters proportionally to the deformation of the images.

In this study the nonrigid registration method could not be fully validated due to the lack of ground truth in creating hemodynamic atlases. Hence, the proposed method was compared only with other registration methods and evaluated using measures such as registration accuracy and interpolation error. Since this was a pilot study to evaluate the method proposed for creating hemodynamic atlases, the study was conducted on a limited number of subjects. Finally, the method was evaluated only for healthy subjects. Future studies should be performed using a larger number of subjects including different patient groups.

In conclusion, this study showed that hemodynamic atlases can be accurately obtained with minimal user interaction using nonrigid registration of 4D Flow MRI. The hemodynamic atlases can add to the pathophysiological understanding of a wide range of cardiac diseases, and can facilitate comparison between individual subjects or groups of subjects.

Acknowledgments

Contract grant sponsor: ERC; contract grant number: Heart4flow, 310612; Contract grant sponsor: Swedish Research Council; contract grant number: 621-2014-6191; Contract grant sponsor: Swedish Heart and Lung Foundation; contract grant number: 20140398.

References

1. Zajac J, Eriksson J, Dyverfeldt P, Bolger AF, Ebbers T, Carlhall C-J. Turbulent kinetic energy in normal and myopathic left ventricles. *J Magn Reson Imaging* 2015;41:1021-1029.
2. Dyverfeldt P, Kvitting JPE, Carlhall CJ, et al. Hemodynamic aspects of mitral regurgitation assessed by generalized phase-contrast MRI. *J Magn Reson Imaging* 2011;33:582-588.
3. Calkoen EE, Roest AA, Kroft LJ, et al. Characterization and improved quantification of left ventricular inflow using streamline visualization

- with 4DFlow MRI in healthy controls and patients after atrioventricular septal defect correction. *J Magn Reson Imaging* 2015;41:1512–1520.
4. Mohiaddin RH. Flow patterns in the dilated ischemic left ventricle studied by MR imaging with velocity vector mapping. *J Magn Reson Imaging* 1995;5:493–498.
 5. Gharib M, Rambod E, Kheradvar A, Sahn DJ, Dabiri JO. Optimal vortex formation as an index of cardiac health. *Proc Natl Acad Sci U S A* 2006;103:6305–6308.
 6. Bermejo J, Benito Y, Alhama M, et al. Intraventricular vortex properties in nonischemic dilated cardiomyopathy. *Am J Physiol Heart Circ Physiol* 2014;306:H718–729.
 7. Poh KK, Lee LC, Shen L, et al. Left ventricular fluid dynamics in heart failure: echocardiographic measurement and utilities of vortex formation time. *Eur Heart J Cardiovasc Imaging* 2012;13:385–393.
 8. Svalbring E, Fredriksson A, Eriksson J, et al. Altered diastolic flow patterns and kinetic energy in subtle left ventricular remodeling and dysfunction detected by 4D Flow MRI. *PLoS One* 2016;11:e0161391.
 9. Nogami Y, Ishizu T, Atsumi A, et al. Abnormal early diastolic intraventricular flow 'kinetic energy index' assessed by vector flow mapping in patients with elevated filling pressure. *Eur Heart J Cardiovasc Imaging* 2013;14:253–260.
 10. Fenster BE, Browning J, Schroeder JD, et al. Vorticity is a marker of right ventricular diastolic dysfunction. *Am J Physiol Heart Circ Physiol* 2015;309:H1087–1093.
 11. Kanski M, Arvidsson PM, Töger J, et al. Left ventricular fluid kinetic energy time curves in heart failure from cardiovascular magnetic resonance 4D flow data. *J Cardiovasc Magn Reson* 2015;17:111–111.
 12. Stugaard M, Koriyama H, Katsuki K, et al. Energy loss in the left ventricle obtained by vector flow mapping as a new quantitative measure of severity of aortic regurgitation: a combined experimental and clinical study. *Eur Heart J Cardiovasc Imaging* 2015;16:723–730.
 13. Gurel E, Prinz C, Van Casteren L, Gao H, Willems R, Voigt JU. The impact of function-flow interaction on left ventricular efficiency in patients with conduction abnormalities: a particle image velocimetry and tissue Doppler study. *J Am Soc Echocardiogr* 2016;29:431–440.
 14. Eriksson J, Bolger AF, Ebberts T, Carlhall CJ. Four-dimensional blood flow-specific markers of LV dysfunction in dilated cardiomyopathy. *Eur Heart J Cardiovasc Imaging* 2013;14:417–424.
 15. Al-Wakeel N, Fernandes JF, Amiri A, et al. Hemodynamic and energetic aspects of the left ventricle in patients with mitral regurgitation before and after mitral valve surgery. *J Magn Reson Imaging* 2015;42:1705–1712.
 16. Carlhall CJ, Bolger A. Passing strange: flow in the failing ventricle. *Circ Heart Fail* 2010;3:326–331.
 17. Dyverfeldt P, Bissell M, Barker AJ, et al. 4D flow cardiovascular magnetic resonance consensus statement. *J Cardiovasc Magn Reson* 2015;17.
 18. Markl M, Frydrychowicz A, Kozerke S, Hope M, Wieben O. 4D flow MRI. *J Magn Reson Imaging* 2012;36:1015–1036.
 19. Markl M, Kilner PJ, Ebberts T. Comprehensive 4D velocity mapping of the heart and great vessels by cardiovascular magnetic resonance. *J Cardiovasc Magn Reson* 2011;13:7.
 20. Markl M, Schnell S, Barker AJ. 4D flow imaging: current status to future clinical applications. *Curr Cardiol Rep* 2014;16:481–481.
 21. Markl M, Schnell S, Wu C, et al. Advanced flow MRI: emerging techniques and applications. *Clin Radiol* 2016 [Epub ahead of print].
 22. Stankovic Z, Allen BD, Garcia J, Jarvis KB, Markl M. 4D flow imaging with MRI. *Cardiovasc Diagn Ther* 2014;4:173–192.
 23. Rengier F, Delles M, Eichhorn J, et al. Noninvasive 4D pressure difference mapping derived from 4D flow MRI in patients with repaired aortic coarctation: comparison with young healthy volunteers. *Int J Cardiovasc Imaging* 2015;31:823–830.
 24. van Ooij P, Potters WV, Nederveen AJ, et al. A methodology to detect abnormal relative wall shear stress on the full surface of the thoracic aorta using four-dimensional flow MRI. *Magn Reson Med* 2015;73:1216–1227.
 25. van Ooij P, Potters WV, Collins J, et al. Characterization of abnormal wall shear stress using 4D flow MRI in human bicuspid aortopathy. *Ann Biomed Eng* 2015;43:1385–1397.
 26. Maintz JB, Viergever MA. A survey of medical image registration. *Med Image Anal* 1998;2:1–36.
 27. Xiang QS. Temporal phase unwrapping for CINE velocity imaging. *J Magn Reson Imaging* 1995;5:529–534.
 28. Bustamante M, Gupta V, Carlhall C-J, Ebberts T. 4D Phase-contrast magnetic resonance cardioangiography (4D PC-MRCA) creation from 4D Flow MRI. In: *Medical Image Computing and Computer-Assisted Intervention — MICCAI 2016: 19th International Conference, Athens, Greece, October 17-21, 2016, Proceedings, Part III*. ed. Edited by Ourselin S, Joskowicz L, Sabuncu MR, Unal G, Wells W. Cham, Switzerland: Springer International; 2016: 519–526.
 29. Ordas S OE, Leta R, Carreras F, Frangi AF. A statistical shape model of the heart and its application to model-based segmentation. *Proc SPIE* 2007;6511.
 30. Yushkevich PA, Piven J, Hazlett HC, et al. User-guided 3D active contour segmentation of anatomical structures: significantly improved efficiency and reliability. *Neuroimage* 2006;31:1116–1128.
 31. Knutsson H, Andersson M. Morphons: Segmentation using elastic canvas and paint on priors. *IEEE Image Proc* 2005:2417–2420.
 32. Knutsson H, Andersson M. Morphons: Paint on priors and elastic canvas for segmentation and registration. *Lect Notes Comput Sci* 2005;3540:292–301.
 33. Forsberg D, Andersson M, Knutsson H. Adaptive anisotropic regularization of deformation fields for non-rigid registration using the Morphon framework. *IEEE International Conference on Acoustics, Speech, and Signal Processing* 2010:473–476.
 34. Lorenz R, Bock J, Barker AJ, et al. 4D flow magnetic resonance imaging in bicuspid aortic valve disease demonstrates altered distribution of aortic blood flow helicity. *Magn Reson Med* 2014;71:1542–1553.
 35. Garcia J, Barker AJ, Collins JD, Carr JC, Markl M. Volumetric quantification of absolute local normalized helicity in patients with bicuspid aortic valve and aortic dilatation. *Magn Reson Med* 2016 doi: 10.1002/mrm.26387 [Epub ahead of print].
 36. Steding-Ehrenborg K, Arvidsson PM, Töger J, et al. Determinants of kinetic energy of blood flow in the four-chambered heart in athletes and sedentary controls. *Am J Physiol Heart Circ Physiol* 2016;310:H113–122.
 37. Carlsson M, Heiberg E, Töger J, et al. Quantification of left and right ventricular kinetic energy using four-dimensional intracardiac magnetic resonance imaging flow measurements. *Am J Physiol Heart Circ Physiol* 2012;302:H893–900.
 38. Kilner PJ, Yang GZ, Mohiaddin RH, Firmin DN, Longmore DB. Helical and retrograde secondary flow patterns in the aortic arch studied by three-directional magnetic resonance velocity mapping. *Circulation* 1993;88(5 Pt 1):2235–2247.
 39. Morbiducci U, Ponzini R, Rizzo G, et al. In vivo quantification of helical blood flow in human aorta by time-resolved three-dimensional cine phase contrast magnetic resonance imaging. *Ann Biomed Eng* 2009;37:516–531.
 40. Charonko JJ, Kumar R, Stewart K, Little WC, Vlachos PP. Vortices formed on the mitral valve tips aid normal left ventricular filling. *Ann Biomed Eng* 2013;41:1049–1061.
 41. Elbaz MS, Calkoen EE, Westenbergh JJ, Lelieveldt BP, Roest AA, van der Geest RJ. Vortex flow during early and late left ventricular filling in normal subjects: quantitative characterization using retrospectively-gated 4D flow cardiovascular magnetic resonance and three-dimensional vortex core analysis. *J Cardiovasc Magn Reson* 2014;16:78.